International Journal of Fatigue 37 (2012) 134–145

Contents lists available at SciVerse ScienceDirect

International Journal of Fatigue

journal homepage: www.elsevier.com/locate/ijfatigue

# High resolution analysis of opening and sliding in fatigue crack growth

Michael D. Sangid [a], Garrett J. Pataky [b], Huseyin Sehitoglu [b,*], Reginald F. Hamilton [c], Hans J. Maier [d]

[a] School of Aeronautics and Astronautics, Purdue University, 701 W. Stadium Ave., West Lafayette, IN 47907-2045, USA
[b] Department of Mechanical Science and Engineering, University of Illinois at Urbana-Champaign, 1206 W. Green St., Urbana, IL 61801, USA
[c] Department of Engineering Science and Mechanics, Pennsylvania State University, 212 Earth-Engineering Sciences Bldg., University Park, PA 16802-6812, USA
[d] Lehrstuhl für Werkstoffkunde (Materials Science), University of Paderborn, 33095 Paderborn, Germany

ARTICLE INFO

*Article history:*
Received 14 August 2011
Received in revised form 30 October 2011
Accepted 3 November 2011
Available online 11 November 2011

*Keywords:*
Fatigue crack growth
Mixed mode
Crack closure
Crack opening
Stainless steel

ABSTRACT

The use of digital image correlation analysis during fatigue crack growth (FCG) of polycrystalline and [1 1 1] oriented single crystal specimens of 316L stainless steel allows for the investigation of mixed mode crack propagation in the vicinity of the crack tip. This technique offers significant benefit in addressing crack closure at the microscale compared to the large body of work studying this phenomenon at the macroscale. Understanding of FCG behavior relies on the sliding (mode II) details which can be rather complicated. In this study, the mode I (opening) and mode II (sliding) mechanisms are differentiated within the single crystal specimens for slanted cracks. Further, crack opening displacement profiles are obtained in mode I and mode II, which are used to quantify crack closure in each specimen. Finally, the irreversible strain within the plastic zone ahead of the crack tip is measured during crack propagation. The results show that [1 1 1] oriented single crystal specimen fatigued at $R = -1$ display the most slip irreversibilities due to reverse dislocation motion leading to dislocation kinks/jogs. As a result, residual stress is diminished at the crack tip thereby resulting in earlier crack opening within the loading cycle.


## 1. Introduction

Fatigue crack growth (FCG) remains a critical life-limiting failure mechanism in engineering components. The complexities in understanding the propagation phenomena exist despite the large body of work on the macroscopic characteristics of crack advancement. To simplify the problem at hand, fatigue crack propagation was analyzed in single crystals to grasp the physics of crack advancement. The mechanism of crack growth is dislocation emission from the crack tip, which strongly depends on the orientation of the crystal [1]. In fact, crack propagation is locally affected by the microstructure at the crack tip as crack propagation occurs through successive blunting (during the tensile loading portion) and sharpening (during the reversal of load) of the crack tip [2]. By modeling crack propagation as a series of slip processes, Neumann accurately predicted the crack growth rate of straight cracks with well defined geometry in single crystals [3]. He refined his model to account for elastic anisotropy thereby including inhomogeneity of slip on activated slip bands [4]. In the above studies, pure metals were analyzed, although experiments have been conducted on single crystals of engineering alloys, including stainless steel [5] and Ni-based superalloys [6]. The results showed that cracks grow on {111} slip planes at the microscale, which introduced mixed mode cracking [6]. In the present work, we analyze the mechanism of crack advancement in stainless steel single crystals including mixed mode cracking. Historically, measuring mode II crack growth, i.e. sliding, has proven to be difficult [7]. By the use of high resolution digital image correlation (DIC) and single crystal specimens, however, we are now able to quantify the effects of mixed mode crack growth.

In 1961, Forsyth recognized that stage I cracks sustained opening and sliding displacements, thus introducing the need to study mode II crack growth [8]. Typically, in polycrystals, stage II cracks grow at 90° with respect to the external load axis, thus representing pure mode I, i.e. opening; whereas, stage I cracks grow at 45° due to deformation along slip bands, thus combining modes I and II propagation [2] and requiring a combination of mixed mode stress intensity factors for analysis and life prediction [9]. Starting in the late 1970s and 1980s, many experimental studies focused on mixed mode crack growth, which suggested that crack growth is governed by local tensile stresses and shear stresses at the crack tip, generally resulting in in-plane loading conditions [7,9–11]. Many variables and parameters influence mixed mode crack growth, including load magnitudes, material strength, initial crack tip conditions, e.g. pre-cracking method, mean stress (or cyclic stress ratio), overloads, crack tip plasticity, and crack closure [12,13]. Of primary importance to the crack propagation rate is the role of crack closure, which is analyzed in this study utilizing high resolution displacement measurement.

* Corresponding author.
*E-mail address:* huseyin@illinois.edu (H. Sehitoglu).

0142-1123/$ - see front matter © 2011 Elsevier Ltd. All rights reserved.
doi:10.1016/j.ijfatigue.2011.11.001

In 1963, Christensen reported roughness-induced crack closure during FCG [14]. When the crack paths are tortuous, there is a significant sliding component at the crack tips that modifies crack advancement. Elber, in 1970, discussed the impact of plasticity-induced crack closure as it influences the effective fatigue crack propagation rate [15]. He noted that cracks remain shut during a portion of the tensile loading cycle, thus this portion of loading does not promote crack advancement and should not be incorporated into calculations of the stress intensity factor range, $\Delta K$ [16]. Crack closure is ultimately due to the reversal of strain at the crack tip, which plays a critical role in the crack propagation mechanism. During crack closure, there is a reversal of dislocation motion, which can remove the residual stress produced during crack opening while leaving the newly formed crack surface intact [4]. This effectively restarts the process to allow the crack to continue propagating during the next loading cycle. Many parameters influence the phenomenon of plasticity-induced crack closure; in order to explain these variables in a unified manner, finite element based analysis was used to explain the role of material constraint, applied stress, strain hardening, mean stress, crack size, and notch effects on fatigue crack growth behavior [17,18]. By accounting for crack closure, the FCG rates condense to a single curve in single crystal specimens with various loading orientations [6]. Thus, there is a strong need to account for crack closure, although accurately measuring crack closure is not a simple task.

Elber measured crack closure using displacement gages [15,16]. This technique has progressed to include back-face strain gages, crack mouth gages, and clip gages [19]. Other methods include electrical potential drop [20] or replica techniques [21]. Non-contact methods emerged which allowed for in situ measurements without disturbing the test specimen including laser interferometric displacement gages [22] and DIC techniques [23,24]. Stereo-imaging analysis allows for displacement and strain measurements at the crack tip [25,26]. This study adopts the methodology of collecting data in real time over many cycles for full-field measurements of crack closure to accurately predict crack opening levels [27]. In this study, we use high resolution DIC to quantify crack closure levels and also study the crack displacement and strain fields at the crack tip. These local crack tip measurements allow us to distinguish opening (mode I) and sliding (mode II) crack growth and also quantify the slip irreversibility process at the crack tip in polycrystalline and single crystal specimens.

The physics of crack advancement are directly influenced by the interaction of dislocations emitted from the crack tip with the local microstructure (in the vicinity of the crack tip), which can lead to complex dislocation arrangements. The result of this process is slip irreversibilities during fatigue loading. The slip introduced during forward loading is not recovered fully during reverse loading due to the following: activation of different slip systems, cutting of dislocations, annihilation of edge dislocations producing vacancies, cross-slipping of screw dislocations, shearing of precipitates, the presence of grain boundaries (in polycrystalline samples), etc. Hence, fatigue damage and crack propagation is governed by irreversible plastic flow [28]. Mughrabi quantified the cyclic slip irreversibility $p$, defined as the fraction of plastic shear strain that is microstructurally irreversible [29]. In this case, $p$ varies from 0, as is the case in low loading amplitudes, to 1, for high loading amplitudes and near stress concentrators such as the crack tip. Applying this concept to FCG, Wu et al. presented a model based on a restricted slip reversal process. Their dislocation based approach related the FCG rate to the difference between the average plastic strain ahead of the crack tip during loading and unloading [30]. Advanced models such as discrete dislocation dynamics [31] and cohesive zone element [32] have been used to describe FCG, each containing a representation of slip irreversibility thus aiding the FCG process.

It has previously been established that single crystal specimens can shed light onto the fatigue crack growth process without the presence of complicated microstructural features, such as grain boundaries. In this study, we contrast FCG in single crystal and polycrystalline specimens. In the [1 1 1] oriented single crystals, the cracks grow at an angle, thus making it necessary to decompose the crack growth process into mode I (opening) and mode II (sliding). The use of DIC allows us to analyze the crack tip opening profiles, the effects of crack closure, and the role of slip irreversibilities ahead of the crack tip. Each of these phenomena elucidates the physics of crack advancement through careful considerations of the dislocation mechanics and strain fields ahead of the crack tip.

## 2. Experimental details

### 2.1. Material and fatigue testing

In this study, polycrystalline and [1 1 1] oriented single crystal specimens of 316L stainless steel were used for FCG testing. The mechanical behavior of these specimens can be found in [33]. A portion of the material was grown into a single crystal from a seed using the Bridgman technique in vacuum and its orientation was verified using electron backscatter diffraction. Single edge-notch tension specimens were electrical discharge machined with a notch depth of 0.5 mm, a gage length of 9 mm long, a width of 3 mm, and a thickness reported in Table 1. The notch length is included in all reported crack lengths in this study. The specimens were mechanically polished to a mirror finish using abrasive paper up to 2400 grit size. A fine layer of black paint was airbrushed onto each specimen to create a speckle pattern for DIC. An IMI 202FT digital camera was used to capture images during the fatigue crack growth experiments with the magnification, resolution, and measurement frequency as shown in Table 1 for each specimen.

The specimens were cyclically loaded in a servo-hydraulic load frame at the R-ratios and stress ranges given in Table 1 at a rate between 3 and 10 Hz to initiate a crack at the notch. Images of the fatigue crack growth through the [1 1 1] oriented single crystal and polycrystalline specimens are shown in Fig. 1a–c. Once a crack was visually identified, measurement cycles were run periodically to capture a greater number of images per cycle to provide an in-depth analysis into the fatigue process.

### 2.2. Digital image correlation procedure

The results obtained from digital image correlation are used as the basis for each of the analytical techniques in this paper. Since

**Table 1**
Summary of the fatigue crack growth test parameters, specimen dimensions, and imaging parameters.

| Crystallography | R-ratio | Stress range, $\Delta\sigma$ (MPa) | Thickness (mm) | Magnification | Resolution (μm/pix) | Measurement frequency (Hz) | Images per cycle |
|---|---|---|---|---|---|---|---|
| [1 1 1] Single Crystal | 0.05 | 178 | 1.03 | 4.6× | 0.95 | 1 | 15 |
| Polycrystalline | 0.0624 | 245 | 1.23 | 4.9× | 0.90 | 1 | 15 |
| [1 1 1] Single crystal | −1 | 300 | 1.75 | 6× | 0.78 | 0.08 | 188 |

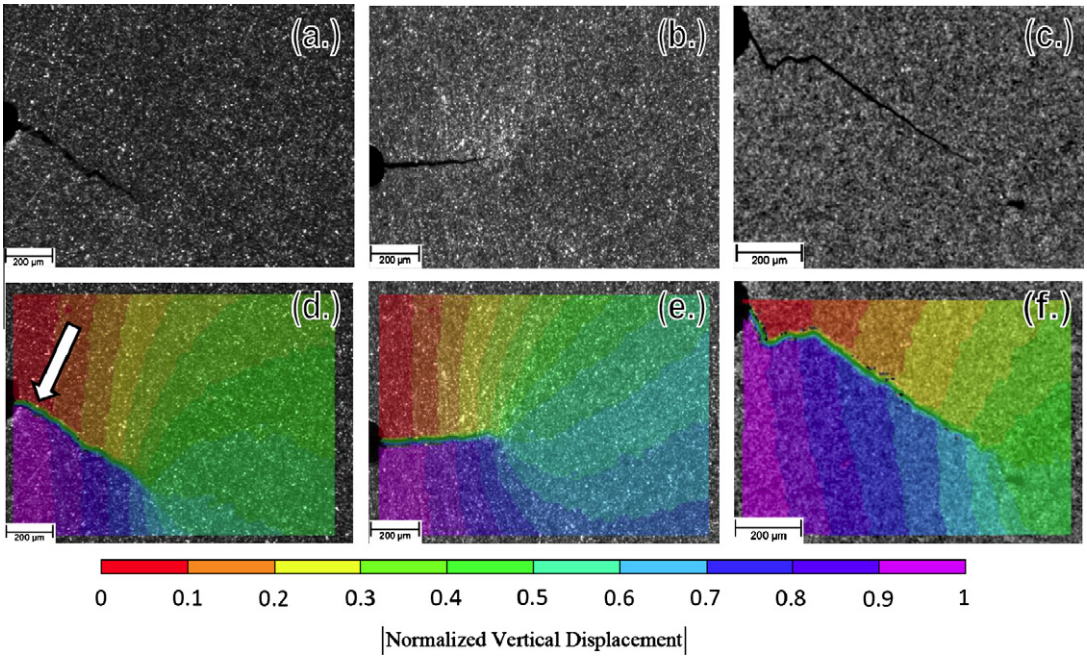


**Fig. 1.** Snapshots recorded during the fatigue crack growth experiments of: (a) [1 1 1] oriented single crystal specimen at $R = 0.05$ and $\Delta\sigma = 178$ MPa, (b) a polycrystalline specimen at $R = 0.0624$ and $\Delta\sigma = 245$ MPa, and (c) [1 1 1] oriented single crystal specimen at $R = -1$ and $\Delta\sigma = 300$ MPa. Vertical displacement contours of each specimen are shown using digital image correlation, which are normalized by the maximum displacement measured in each specimen. The images in (d), (e), and (f) correspond to the specimens and experimental parameters in (a), (b), and (c), respectively. In (d) the arrow points to the location of a carbide particle, which deflected the crack thus influencing the crack closure at this location.

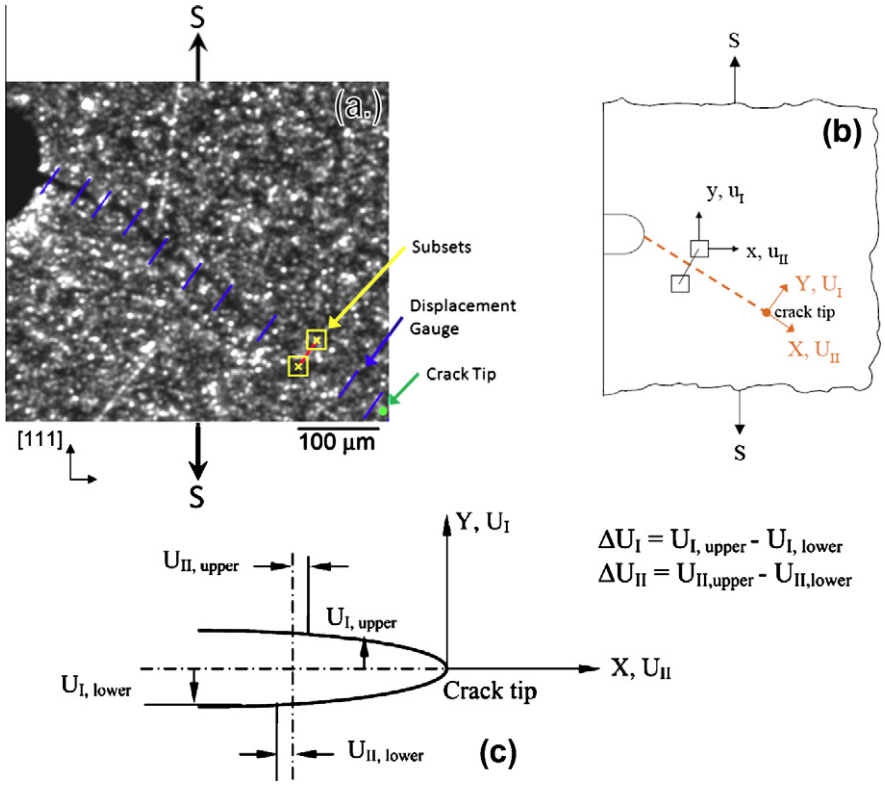


**Fig. 2.** (a) An example of the two-subset virtual extensometers on the [1 1 1] oriented specimen. Each line across the crack represents a different extensometer. The subsets on each side of the crack, as pointed out by an arrow, will separate as the crack opens. (b) A schematic showing the displacements measured by the extensometers. (c) Coordinate system for measuring crack opening and sliding displacement.

DIC compares the light intensity on the surface of a deformed image to that of a reference image to determine the displacements, a random array of intensity levels is necessary, typically created using a speckle pattern. The surface contains numerous pixels of

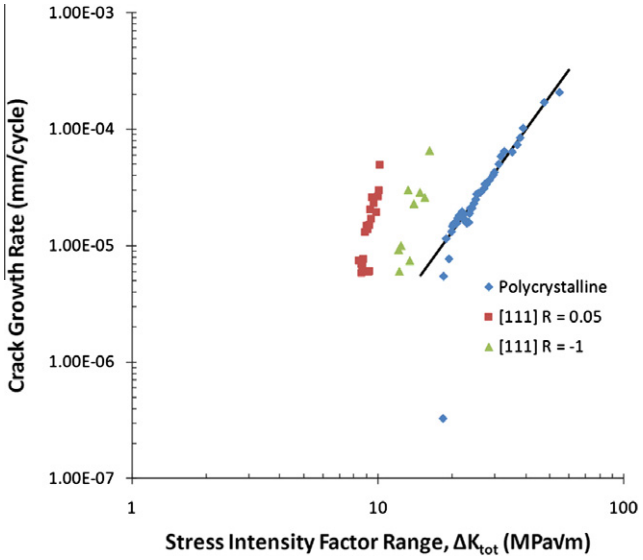


**Fig. 3.** Fatigue crack growth results for the polycrystalline and single crystal 316L SS specimens at room temperature in air with test conditions shown in Table 1. The Paris law fit is shown for the polycrystalline specimen and the coefficients for the Paris law fits and threshold stress intensity factor for each specimen are summarized in Table 2.

**Table 2**
Paris law constants and stress intensity factor threshold from fatigue crack growth tests of 316L SS.

| Crystallography | R-ratio | $\Delta K_{thres}$ (MPa$\sqrt{}$m) | $C$ | $m$ |
|---|---|---|---|---|
| [1 1 1] Single crystal | 0.05 | 20 | $9.96 \times 10^{-13}$ | 7.46 |
| Polycrystalline | 0.0624 | 18 | $3.64 \times 10^{-10}$ | 3.43 |
| [1 1 1] Single crystal | −1 | 21 | $7.86 \times 10^{-13}$ | 6.45 |

the varying light intensity and square groups of pixels, or subsets, define unique blocks of light intensities. DIC uses an initial guess and finds the displacements by tracking individual subsets and determining the best correlation between the two images. A commercially available image correlation program (Vic-2d produced by Correlated Solutions) performed DIC during the measurement cycles. The first image of each measurement cycle, captured at minimum load, was used as the reference image for that cycle including the full image field, both behind and ahead of the crack tip. The maximum subset size was 72 μm by 72 μm with a maximum of 9 μm between the centers of the subsets. At each correlated point, the horizontal ($\Delta x$) and vertical ($\Delta y$) displacements were calculated and differentiated to obtain the strains assuming a small strain approximation. Localized smoothing of the strain was performed by the built-in filtering function in Vic-2D. Images of the vertical displacement, $\Delta y$, contours are shown for each specimen in Fig. 1d and f. Using DIC, so called two-point virtual extensometers can be defined, which track two subsets, one on each side of the crack flanks, as shown in Fig. 2a and b. By using the first image in the cycle as the reference image, the load level at which the crack begins to open is identified. Since the virtual extensometers require no physical setup, many of these can be placed along the crack face, as displayed in Fig. 2a, thus allowing for distinctions between the global and crack tip crack closure. The virtual extensometers must be placed perpendicular to the crack flanks, in order to get the pure vertical ($\Delta U_I$) and horizontal ($\Delta U_{II}$) displacements. Once completed, the advantage of using the virtual extensometers is the clear distinction between the two types of displacements without needing to rotate any of the processed data, as shown in Fig. 2c. This makes it easy to analyze mixed mode fatigue crack growth. The difference in the vertical crack tip displacements, $\Delta U_I = \Delta U_{I,upper} - \Delta U_{I,lower}$, describes the mode I crack opening, and the horizontal crack tip displacements, $\Delta U_{II} = \Delta U_{II,upper} - \Delta U_{II,lower}$, describes the mode II crack sliding. The gages are placed starting at 20 μm in front of the crack tip and extended back behind the crack until the notch was reached, thus allowing for crack opening displacement profile measurements during loading.

### 2.3. Transmission electron microscopy procedure

For transmission electron microscopy (TEM) 1 mm thick discs were sectioned with a low-speed diamond saw parallel to the loading axis from the failed specimens, and then mechanically ground and polished down to 0.15 mm foil thickness. Large electron transparent areas were obtained in these foils by conventional twin jet polishing using a solution consisting of 5 pct perchloric acid in ethanol at −20 °C and 15 V. The TEM was operated at a nominal voltage of 200 kV and a double-tilt specimen holder was employed for imaging under two-beam conditions.

## 3. Results

### 3.1. Fatigue crack growth

Fatigue crack growth tests were performed on a polycrystalline specimen and two single crystal specimens oriented in the [1 1 1] crystallographic direction. The crack growth behavior as a function of the total stress intensity range is given in Fig. 3. The stress intensity factor ranges displayed were determined using:

$$\Delta K_I = \Delta\sigma\sqrt{\pi a} \times f(a/w) \tag{1}$$

$$\Delta K_{II} = \Delta\tau\sqrt{\pi a} \times f(a/w) \tag{2}$$

where $\Delta\sigma$ and $\Delta\tau$ are the normal and shear stress ranges on the crack plane, respectively, $a$ is the crack length, and $f(a/w)$ is the geometric correction factor. The stress intensity factors were measured in MPa$\sqrt{m}$. For a single-edge notch tension specimen, the geometric correction factor is given as [34]:

$$f(a/w) = 0.265(1 - a/w)^4 + \frac{0.857 + 0.265(1 - a/w)}{(1 - a/w)^{3/2}} \tag{3}$$

where $a$ is the crack length and $w$ is the specimen width.

The most general expression for combining the stress intensity factor ranges to calculate $\Delta K_{tot}$ is given as follows [9].

$$\Delta K_{tot} = \sqrt{\Delta K_I^2 + \alpha \cdot \Delta K_{II}^2} \tag{4}$$

Since the anisotropic case is complex, it requires the use of the energy release rates, $\Im_i$, Eqs. (5) and (6) for mode I and mode II, respectively [35]. The ratio between these two energy release rates is used to calculate $\alpha$, i.e. $(\alpha = \Im_1/\Im_2)$

$$\Im_1 = -\frac{\pi K_I}{2} a_{22} \mathrm{Im}\left[\frac{K_I(\mu_1 + \mu_2) + K_{II}}{\mu_1\mu_2}\right] \tag{5}$$

$$\Im_2 = \frac{\pi K_{II}}{2} a_{11} \mathrm{Im}[K_{II}(\mu_1 + \mu_2) + K_I\mu_1\mu_2] \tag{6}$$

where $a_{ij}$ are the compliance coefficients and $\mu_1$ and $\mu_2$ are the roots found from the characteristic equation for which the imaginary parts are positive.

$$a_{11}\mu^4 - 2a_{16}\mu^3 + (2a_{12} + a_{66})\mu^2 - 2a_{26}\mu + a_{22} = 0 \tag{7}$$

The energy release rate ratio, $\alpha$, ranged from 2.25 to 3.8 for the cases included in this study. Once $\alpha$ was determined, the mixed mode stress intensity factor range, $\Delta K_{tot}$, was calculated and the results are plotted in Fig. 3. The data were fit to the Paris law:

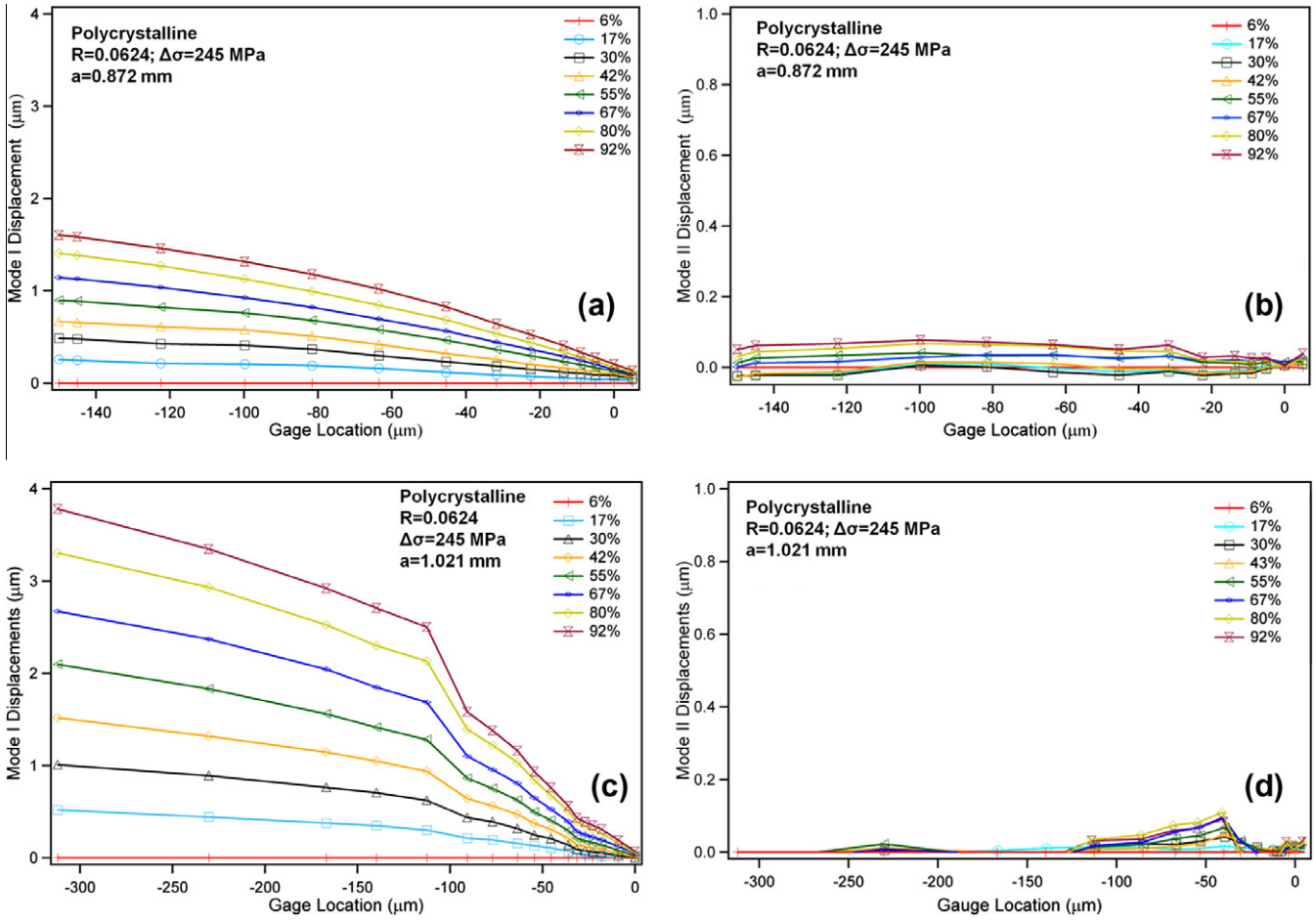


**Fig. 4.** The crack opening displacement profiles of the polycrystalline 316L SS specimen at $R = 0.0624$ and $\Delta\sigma = 245$ MPa: (a) and (c) show the mode I (opening) displacements at crack lengths of 0.872 mm and 1.021 mm, respectively, while (b) and (d) display the mode II (sliding) displacements at crack lengths of 0.872 mm and 1.021 mm, respectively.

$$\frac{da}{dN} = C(\Delta K_{tot})^m = C(\Delta K_I^2 + \alpha \cdot \Delta K_{II}^2)^{m/2} \quad (8)$$

where the Paris law constants $C$ and $m$ are given in Table 2. The crack growth rate, $da/dN$, was measured in mm/cycle. Most of the points captured during the FCG testing occurred in regime II, the steady state region, although the values of the threshold stress intensity factor, $\Delta K_{thres}$, are also reported in Table 2. The Paris exponent, $m$, ranges from 3.43 to 7.46. This is an extremely wide range of values and makes it difficult to characterize the material's fatigue crack growth behavior. Part of the difference in Paris exponent values is due to the comparisons of single crystal and polycrystalline specimens; hence, the microstructure and orientation play a role in the fatigue crack growth rate. Additionally, the scatter observed within each specimen is related to resolution of the images used for the crack tip identification. Low $m$ value implies a slip dominated process while high $m$ values point to the presence of cleavage effects and tensile decohesion [1]. The results show that the two [1 1 1] oriented single crystal specimens (mixed mode I and II) exhibited much lower threshold stress intensity factor ranges to propagate cracks compared to the polycrystalline specimen (pure mode I).

### 3.2. Crack closure

Both the horizontal and vertical displacements for each virtual extensometer were recorded during the entire loading portion of the fatigue cycle. By using the displacement profiles along the entire crack length, the mode I and mode II opening levels were identified. Fig. 4 displays the results for the polycrystalline specimen. Fig. 4a contains the mode I displacements for a crack size of 0.872 mm; the crack begins to open at 17% of the maximum load starting from the notch; whereas, the crack tip opening becomes evident at nearly 30% of the maximum load. As the crack advances, Fig. 4c, the mode I displacements near the notch are more than twice that of the smaller crack length. The crack tip opens at a value similar to the shorter crack case. The steep opening starting at the point 90 μm behind the crack tip is attributed to a small crack redirection at that location, which affects the crack closure levels. As expected due to the crack growing perpendicular to the applied loading and thus experiencing pure mode I conditions, Fig. 4b and d shows nearly zero mode II displacements. The effect of crack redirection is evident in Fig. 4d.

The crack opening displacement profiles for the [1 1 1] oriented single crystal loaded at a load ratio $R$ of 0.05 are shown in Fig. 5. Mixed mode I and II displacements are expected due to the fatigue crack propagating at an angle. During this fatigue crack growth experiment, the crack encountered a carbide particle (Fig. 1d), which affected the crack closure, as observed in Fig. 5a and b. It is seen that the mode I displacements (Fig. 5a) remain shut until 50 μm behind the crack tip, and then open between 43% and 56% of the maximum load. By contrast, the mode II displacements (Fig. 5b) appear to slide at the crack tip between 18% and 31% of the maximum load. As the crack extended to a length of 1.622 mm, roughly 0.1 mm away from

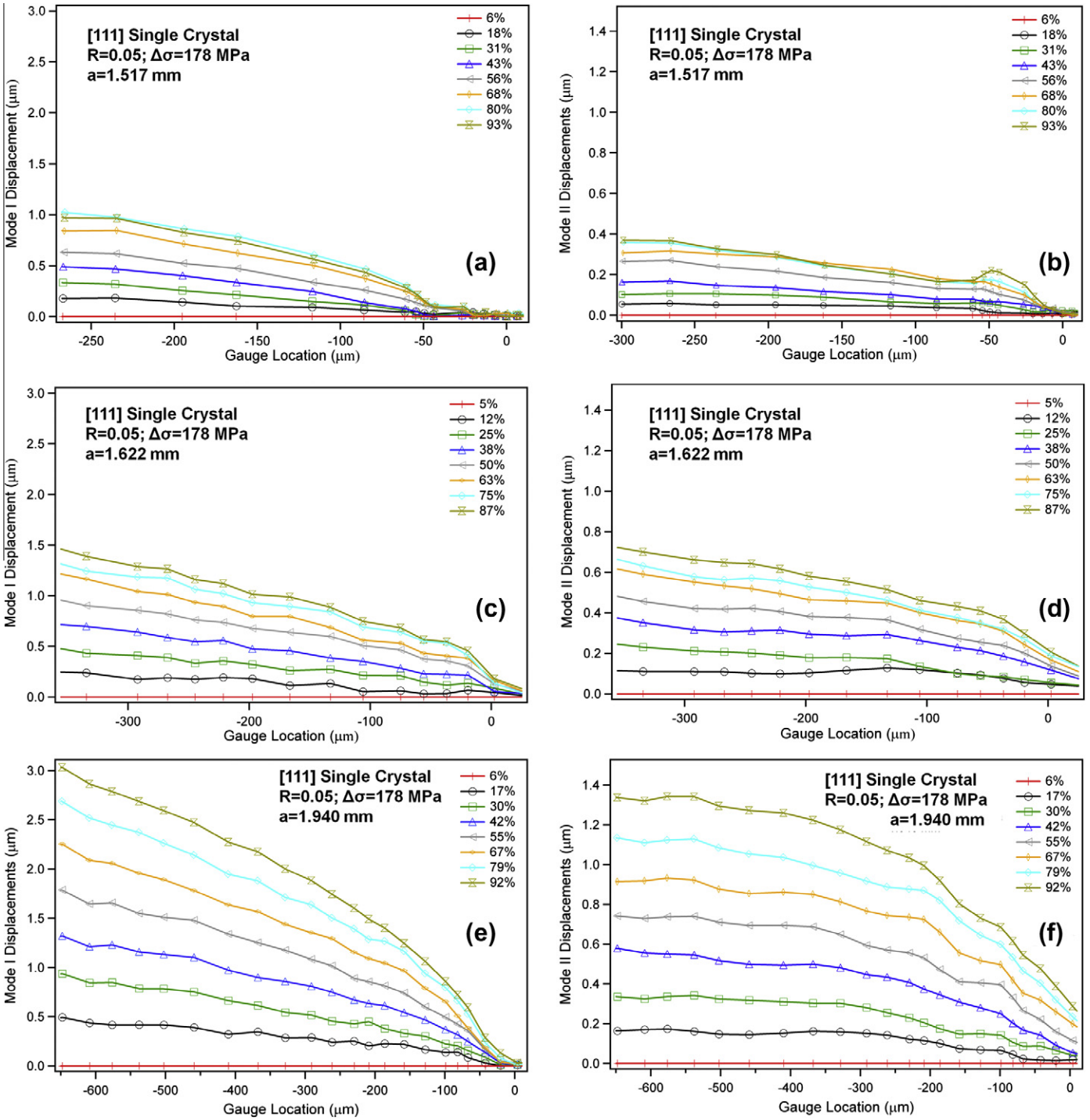


**Fig. 5.** The crack opening displacement profiles of the [1 1 1] oriented single crystal 316L SS specimen at $R = 0.05$ and $\Delta\sigma = 178$ MPa: (a), (c), and (e) show the mode I (opening) displacements at crack lengths of 1.517 mm, 1.622 mm, and 1.940 mm, respectively, while (b), (d), and (f) display the mode II (sliding) displacements at crack lengths of 1.517 mm, 1.622 mm, and 1.940 mm, respectively.

the previous crack opening displacement profiles, the effects of the carbide disappear. As seen in Fig. 5c and d, the crack opens or is fully slipped between 12% and 25%, which matches the results found using finite element models [18]. The largest crack length, 1.940 mm, has the largest displacements in both mode I (Fig. 5e) and mode II (Fig. 5f). The displacements are positive at the crack tip at higher loads in Fig. 5f, which indicated that the crack flanks slid past the initial crack tip location.

The other [1 1 1] oriented single crystal specimen loaded at a load ratio $R$ of $-1$ is observed to have the greatest crack opening displacements, as shown in Fig. 6. Note that the scale is at least twice that of the previous figures. Examining the first crack length of 1.327 mm, the maximum crack flank opening displacements in Fig. 6a are observed to be approximately 4 μm, which is significantly more than the largest crack length of the [1 1 1] oriented specimen subjected to a load ratio $R$ of 0.05. Another interesting observation is that

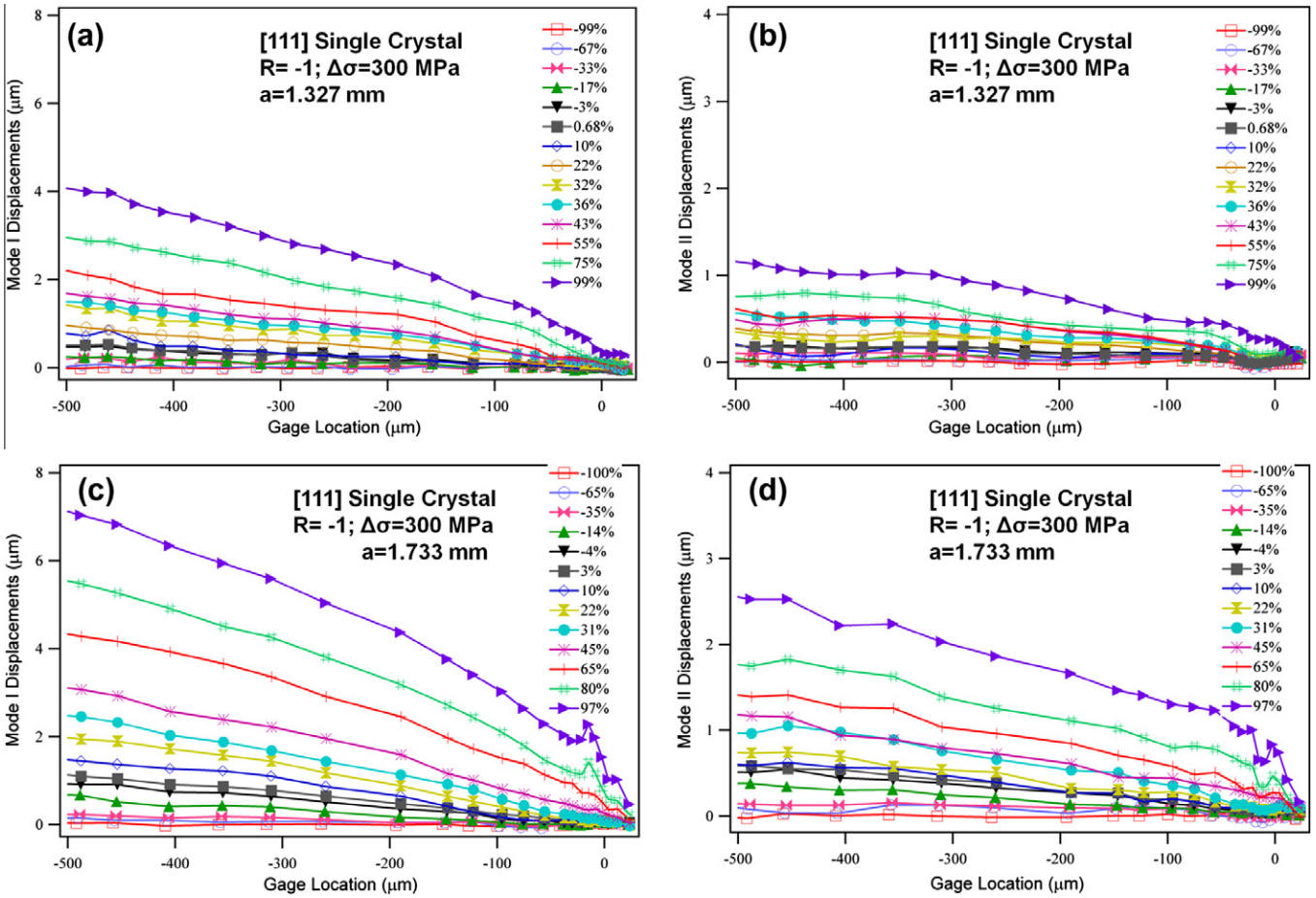


**Fig. 6.** The crack opening displacement profiles of the [1 1 1] oriented single crystal 316L SS specimen at $R = -1$ and $\Delta\sigma = 300$ MPa: (a) and (c) show the mode I (opening) displacements at crack lengths of 1.327 mm and 1.733 mm, respectively, while (b) and (d) display the mode II (sliding) displacements at crack lengths of 1.327 mm and 1.733 mm, respectively. Note that the scale in (a) and (c) is twice that of Fig. 4.

Fig. 6b and d shows that the crack is fully slipped in mode II while still in compression. For the [1 1 1] specimens, at similar crack sizes, the $R = -1$ specimen has a crack opening displacement of approximately 5× the value of the $R = 0.05$ specimen.

## 4. Discussion

### 4.1. Crack opening and sliding

Using the crack opening displacement profiles, the crack closure phenomena in both mode I and mode II were measured as discussed in Section 3.2 and summarized in Fig. 7. These measurements allow us to differentiate and quantify the effects of crack opening (mode I) and sliding (mode II). Their displacements and measuring techniques are sketched in Fig. 7a. The results for the polycrystalline sample loaded in mode I (Fig. 7b) and both of the mode I results for the [1 1 1] oriented single crystals (Fig. 7c and d) indicate that the cracks were closed for approximately 20% of the tensile loading cycle except in the presence of the carbide particle. The effects of the carbide are evident in Fig. 7c with the crack being shut in mode II for the majority of the loading cycle, nearly 60%, after passing the carbide. The results for mode I show that the carbide had a much smaller effect in this case as there exists only as small drop in crack opening level. In the polycrystalline specimen (Fig. 7b), the crack is perpendicular to the applied loaded, and hence only a single opening mode is observed. In all of the crack opening plots in Fig. 7, a trend exists such that a larger value of crack opening displacement is observed with increasing crack length. This is as expected as a larger crack creates less compliance, which facilitates crack opening; exceptions to this trend are present at the site of the carbide (Fig. 7c).

We note substantial differences in the opening character between the two [1 1 1] oriented single crystal specimens. First, the mode I opening level is significantly greater in the $R = -1$ specimen. Additionally, the mode II opening levels in the $R = -1$ specimen shows that the crack opened consistently during the compressive portion of the loading cycle. The major difference in loading between the two [1 1 1] specimens is the compression portion of the fatigue cycle in one of the samples; it was concluded that loading in compression causes the crack to open earlier in the loading cycle and to a greater extent in tension, which is due to the removal of the residual stress at the crack tip during reversed plasticity in the $R = -1$ specimen [4]. This indicates that cyclic loading with a compressive portion of the fatigue cycle is more damaging than that of pure tension cycling.

### 4.2. Crack closure effects on fatigue crack growth

As a consequence of crack closure, the crack opens for only a portion of the loading cycle, and thus acts as a shielding mechanism for stress, which reduces the effective stress intensity factor range at the crack tip to

$$\Delta K_{\text{eff}} = K_{\max} - K_{\text{open}} \tag{9}$$

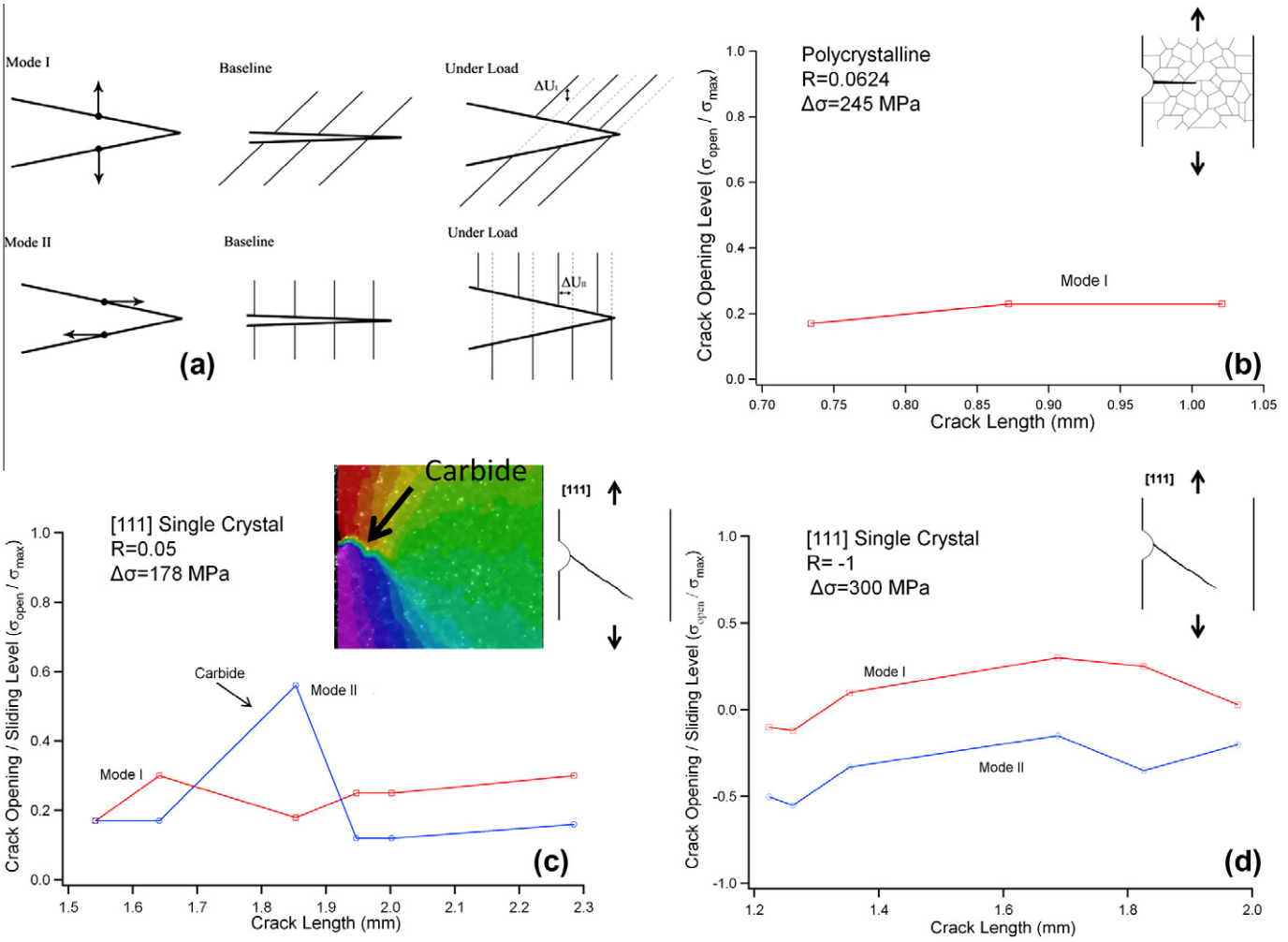


**Fig. 7.** (a) Schematic depicting crack displacement during mode I (opening) and mode II (sliding) crack growth including the unloaded (baseline) and loaded view of the crack. The mode I and mode II crack opening and sliding levels as a function of crack length for (b) polycrystalline specimen, which experiences pure mode I opening due to the horizontal growth of the crack, (c) [1 1 1] oriented single crystal specimen at $R = 0.05$, notice the crack deflection at the carbide particle resulted in an increase in crack sliding, and (d) [1 1 1] oriented single crystal specimen at $R = -1$.

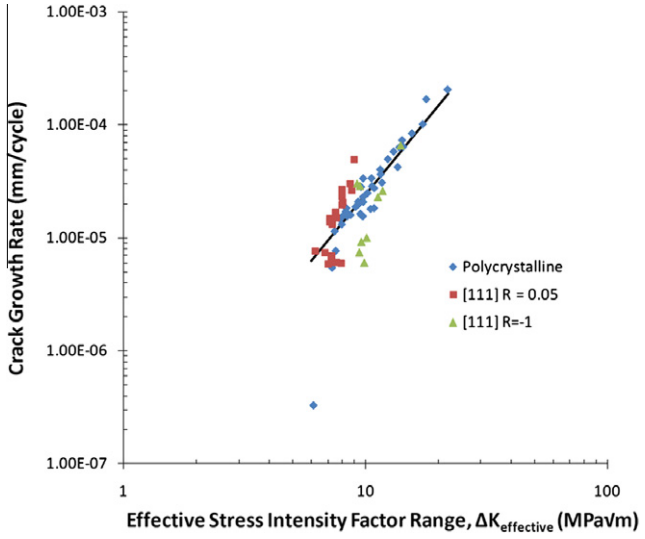


**Fig. 8.** Fatigue crack growth results for the polycrystalline and single crystal 316L SS specimens at room temperature in air with testing conditions summarized in Table 1. The results shown are for the effective stress intensity factor range by taking into account the effects of crack closure. The Paris law fit is shown for the complete set of test results (polycrystalline specimen and two [1 1 1] oriented single crystal specimens). The coefficients for the effective Paris fit and threshold stress intensity factor for each specimen are displayed in Table 3.

Therefore, the effective stress intensity factor range, $\Delta K_{\text{eff}}$, only accounts for the portion of the stress intensity factor above the crack opening level, $K_{\text{open}}$, which is measured using the DIC virtual extensometers at the crack tip and along the crack.

Since cracks can only grow when they are open, we should expect a lower effective stress intensity factor range, $\Delta K_{\text{eff}}$ (Eq. (9)), compared to $\Delta K_{\text{tot}}$ (Eq. (4)), which is modified thereby reducing the crack growth rate [15,16] as follows:

$$\frac{da}{dN} = C'(\Delta K_{\text{eff}})^{m'} = C'(\Delta K_{\text{I,eff}}^2 + \alpha \cdot \Delta K_{\text{II,eff}}^2)^{m'/2}. \quad (10)$$

By modifying for crack closure, the effective fatigue crack growth results are shown in Fig. 8 and the modified Paris law coefficients, $C'$ and $m'$, are given in Table 3. Notice that the data shift to the left as the stress intensity factor range is reduced according to Eq. (9).

**Table 3**
Effective Paris law constants and stress intensity factor threshold from fatigue crack growth tests by taking into account the role of crack closure in 316L SS.

| Crystallography | R-ratio | $\Delta K_{thres}$ (MPa$\sqrt{}$m) | $C'$ | $m'$ |
|---|---|---|---|---|
| [1 1 1] Single crystal | 0.05 | 8 | $6.37 \times 10^{-09}$ | 3.89 |
| Polycrystalline | 0.0624 | 6 | $1.05 \times 10^{-08}$ | 3.32 |
| [1 1 1] Single crystal | −1 | 10 | $3.29 \times 10^{-09}$ | 3.65 |

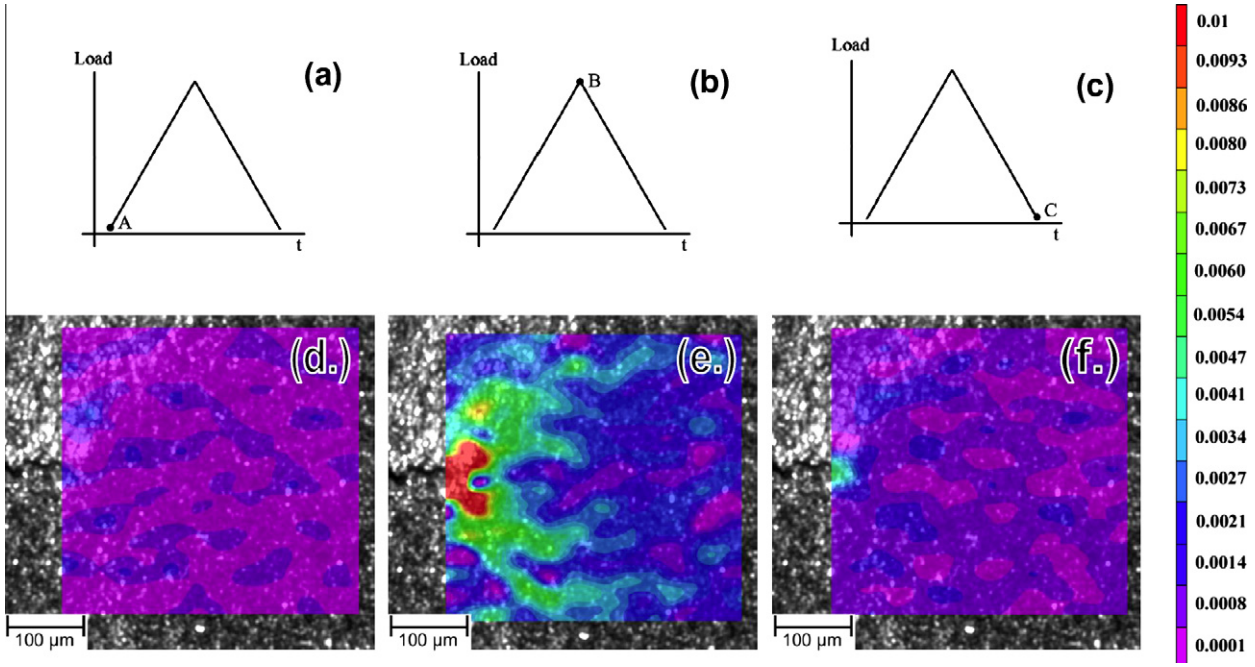


**Fig. 9.** Tensile crack tip strain measurements for the polycrystalline specimen at $R = 0.0624$ and $\Delta\sigma = 245$ MPa, taken at a crack length of 1.239 mm. The strain measurements in (d), (e), and (f) were taken at the three points indicated during the loading cycle in (a), (b), and (c), respectively. The increased contours in (e) and (f) compared to (d) indicate higher strains.

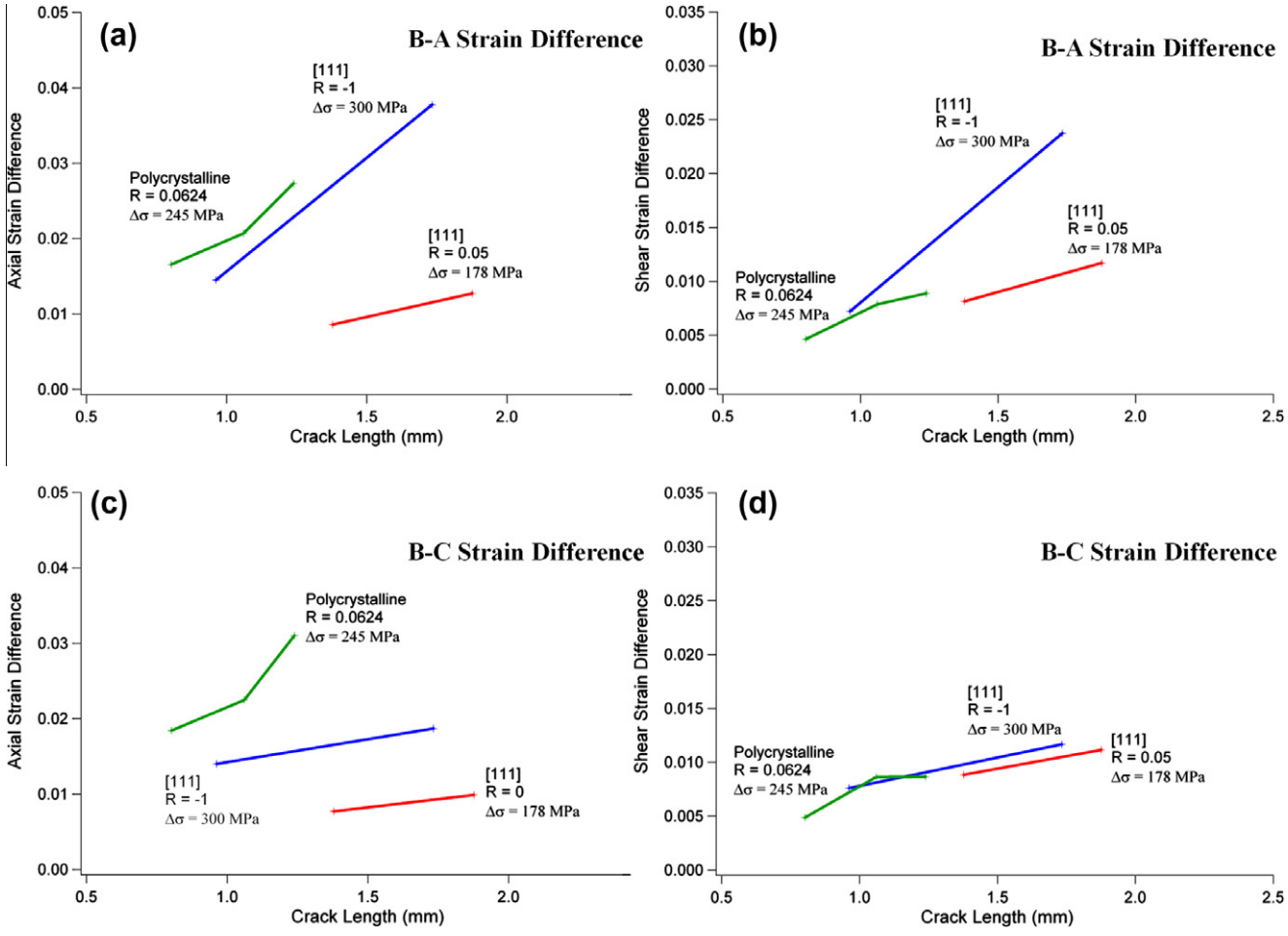


**Fig. 10.** Strain differences during selected loading cycles as a function of crack length for the 316L SS fatigue crack growth specimens. (a) Axial strain differences and (b) shear strain differences between the initial minimum load A and maximum load B. (c) Axial strain differences and (d) shear strain differences between the minimum load at the end of the loading cycle C and the maximum load B. The smaller magnitudes in (c) and (d) as compared to (a) and (b) confirm irreversibility during the cycle.

The threshold values are thus smaller as shown in Table 3, and as a result a smaller crack can start to grow at the same applied stress range. Also, there is a marked decrease in the $m'$ value by accounting for crack closure. As expected, the fatigue crack growth data should consolidate to a single line after taking crack closure into account [6], as shown in Fig. 8. Note that the effective crack growth exponents, $m'$, are nearly the same for all three specimens and have values in the range of 3.32–3.89. Hence, for the [1 1 1] oriented single crystal specimens, the crack closure phenomenon explains the discrepancy in fatigue crack growth rates between the loading conditions, i.e. the loading ratio R. Additionally, by accounting for crack closure, the two single crystal specimens and polycrystalline specimen exhibit the same crack growth rate. Thus, we can measure and isolate the material's resistance to crack growth in the absence of crack closure effects on fatigue crack growth. Moreover, with further analysis of the slip mechanism within the materials and the slip irreversibilities that accumulate during fatigue loading, we can better understand the physics of crack propagation.

### 4.3. Slip mode and irreversibilities

As previously stated, the mechanism for FCG is a series of slip processes, where dislocations are emitted from the crack tip during loading and not fully reversed during unloading. The difference in the average shear strain in the plastic zone ahead of the crack tip during forward and reverse loading is related to the fatigue crack growth rate [30]. Thus, it is important to quantify this concept of slip irreversibility as it relates to the FCG mechanism. In order to gain a quantitative understanding of slip irreversibilities on the mesoscopic scale, we measured strains within the plastic zone ahead of the crack tip during the cyclic loading.

We use DIC to measure the strains within the vicinity of the crack tip at various points in the loading cycle: the minimum load at the beginning of the cycle (Fig. 9a), the maximum load (Fig. 9b), and the minimum load at the end of the cycle (Fig. 9c). The corresponding strain fields are shown in Fig. 9d–f. The strain is measured and averaged within the cyclic plastic zone radius ahead of the crack tip at the minimum load prior to the loading cycle (point A), at the maximum load (point B), and at the minimum load after the completion of the current loading cycle (point C) for each of the three test specimens. The cyclic plastic zone is theoretically one quarter of the monotonic plastic zone size due to reversed loading for an $R = 0$ loading without closure effects [21,36]. The strains were averaged inside this relatively small cyclic plastic zone, which was around the crack tip, to account for the slight strain gradient.

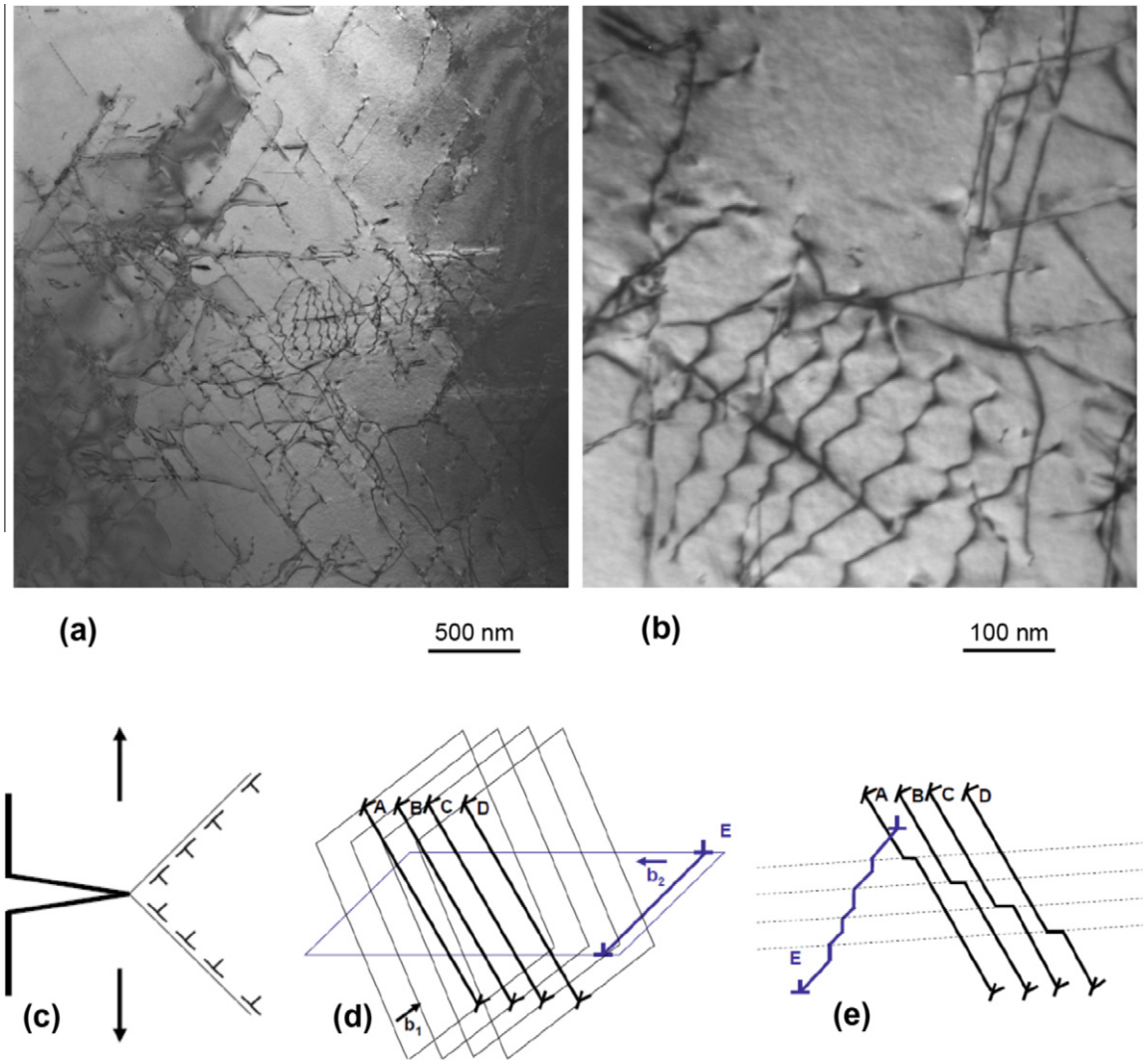


**Fig. 11.** TEM images of the [1 1 1] oriented single crystal specimen showing (a) dislocations present on two slip systems and (b) a network of dislocations formed within the specimen. (c) Schematic of dislocation emission from the crack tip on two slip systems during fatigue loading. (d) The motion of a dislocation on one slip system interacts with present dislocations resulting in (e) cutting of the dislocations and the formation of kinks/jogs.

The $\Delta\varepsilon_{BA}$ value indicates the strain accumulation during the forward loading, which is shown in Fig. 10a for mode I opening (axial strain), and Fig. 10b for mode II (shear strain). The difference between $\Delta\varepsilon_{BA}$ and $\Delta\varepsilon_{BC}$ quantifies the irreversible strain during the complete (forward and reverse) loading cycle as shown in Fig. 10c (axial) and d (shear).

The inequality between the strain differences in the loading, $\Delta\varepsilon_{BA}$, and unloading portions, $\Delta\varepsilon_{BC}$, of the fatigue cycle revealed unrecovered strains, $\Delta\varepsilon_{CA,ir}$, and thus irreversibility. The [1 1 1] oriented single crystal specimen at $R = -1$ exhibited the greatest quantity of irreversibility, $\Delta\varepsilon_{CA,ir}$, in both the axial and shear strain cases, and moreover, this specimen contained the largest amount of crack opening displacement and underwent displacement in the compression region of loading. These findings suggest a tremendous amount of plasticity occurring at and ahead of the crack tip, thereby promoting a large degree of slip irreversibilities. For each specimen, the slip irreversibility increases with increasing crack size, i.e. higher stress intensity ranges, which is in agreement with Mughrabi's quantification [29].

We are able to quantify the amount of forward and reverse slip ahead of the crack tip, which provides us information about the crack tip dislocation mechanics and physics of crack propagation. To further explain the dislocation behavior of the material in the vicinity of the crack tip, we employ TEM analysis. TEM images of the dislocation arrangements in the [1 1 1] oriented single crystal specimen captured near the propagated crack. As we can see in Fig. 11a, dislocations are present on two activated slip systems. Furthermore, from the two slip systems, a network of dislocations forms (Fig. 11b). Typically, during fatigue loading, dislocations are emitted on at least one system during loading and another system during reverse loading [1–3], as shown schematically in Fig. 11c. Hence, it is expected to observe dislocations residing on two active slip systems near the crack, as shown in Fig. 11a and schematically in Fig. 11d. The result of the activation of two slip systems is dislocation-to-dislocation interaction. An emitted dislocation on a given slip plane reacts with the existing dislocations on a different slip plane, thereby cutting the dislocations (Fig. 11e). The results of these interactions are jogs and kinks (depending on the character of the dislocations [37]), exemplified by the dislocation arrangement in Fig. 11b. The compression loading within the [1 1 1] oriented single crystal specimen loaded at $R = -1$ augments the backward motion of the dislocations, thus enhancing dislocation-to-dislocation interactions and increasing the number of jogs and kinks. The greater number of jogs and kinks thereby increases entanglement of the dislocation network and the amount of slip irreversibilities, as seen in Fig. 10 for the [1 1 1] oriented single crystal specimen fatigued at $R = -1$. Our interpretation of the dislocations role in slip irreversibilities further elucidates the physics of crack advancement.

Finally, we note that the stress–strain response ahead of the crack tip plays an important role in the fatigue crack growth rate [38]. Our $K$ calculations are based on the displacement measurements encompassing the entire crack tip domain and reflect the deformation behavior ahead of the crack tip. We also recognize that the crack tip stresses are altered by the closure effects, and the external load levels may need to be increased beyond the opening stress level to render the crack tip tensile. This needs to be addressed in future research.

## 5. Conclusions

This work has outlined considerable progress in the analysis of fatigue crack growth. The major contributions are as follows:

- As demonstrated for [1 1 1] oriented single crystals and polycrystalline 316L stainless steel specimens, digital image correlation allows for precise measurements of the displacement and strain fields during fatigue crack growth.
- The use of the virtual extensometers allows for differentiation of mode I versus mode II crack growth, as mixed mode crack propagation is evident in the [1 1 1] oriented single crystals since the cracks grew inclined with respect to the load axis.
- The mode I crack opening displacement profiles suggest that the cracks are closed for approximately 20% of the tensile loading cycle. Further, when a compressive load is applied, the mode II cracks open earlier within the loading cycle and both modes experience a greater crack tip displacement.
- After accounting for crack closure, the crack growth rates for the [1 1 1] oriented single crystal (of various loading ratios) and polycrystalline specimens consolidate into a single fatigue crack growth curve. Thus, plasticity-induced crack closure plays a critical role in the crack propagation mechanism in this material.
- Slip irreversibilities are quantified in the plastic zone ahead of the crack tip. The [1 1 1] oriented single crystal specimen at $R = -1$ displayed the greatest value of irreversible slip. This suggests that reversal of dislocations during compressive loading intensified dislocation interactions resulting in jogs and kinks.

## Acknowledgments

The research was supported by a Critical Research Initiative (CRI) at the University of Illinois and partly by the US Department of Energy Nuclear Energy University Program (NEUP) under grant DOE-INL-00091210 and a CRDF Award under grant RUE1-2983-TO-10. The authors would like to thank Prof. Yuri Chumlyakov of Siberian Physical-Technical Institute, Russia for providing the single crystal specimens.

## References

[1] McEvily JAJ, Boettner RC. On fatigue crack propagation in F.C.C. metals. Acta Metall 1963;11:725.
[2] Laird C. The influence of metallurgical structure on the mechanisms of fatigue crack propagation. In: Fatigue crack propagation, ASTM STP 415. Philadelphia, PA: American Society of Testing and Materials; 1967. p. 131–80.
[3] Neumann P. New experiments concerning the slip processes at propagating fatigue cracks–I. Acta Metall 1974;22:1155.
[4] Neumann P. The geometry of slip processes at a propagating fatigue crack–II. Acta Metall 1974;22:1167.
[5] Rieux P, Driver J, Rieu J. Fatigue crack propagation in austenitic and ferritic stainless steel single crystals. Acta Metall 1979;27:145.
[6] Chan KS, Hack JE, Leverant GR. Fatigue crack growth in MAR-M200 single crystals. Metall Trans A (Phys Metall Mater Sci) 1987;18A:581.
[7] Smith MC, Smith RA. Toward an understanding of mode II fatigue crack growth. In: Basic questions in fatigue: vol. I, ASTM STP 924. Philadelphia, PA: American Society of Testing and Materials; 1988. p. 260–80.
[8] Forsyth PJE, Ryder DA. Some results of examination of aluminium alloy specimen fracture surfaces. Metallurgia 1961;63:117.
[9] Tanaka K. Fatigue crack propagation from a crack inclined to the cyclic tensile axis. Eng Fract Mech 1974;6:493.
[10] Otsuka A, Mori K, Miyata T. The condition of fatigue crack growth in mixed mode condition. Eng Fract Mech 1975;7:429.
[11] Gao H, Alagok N, Brown MW, Miller KJ. Growth of fatigue cracks under combined mode I and mode II loads. In: Multiaxial fatigue, ASTM STP 853. Philadelphia, PA: American Society of Testing and Materials; 1985. p. 184–202.
[12] Qian J, Fatemi A. Mixed mode fatigue crack growth: a literature survey. Eng Fract Mech 1996;55:969.
[13] Bold PE, Brown MW, Allen RJ. Review of fatigue crack growth in steels under mixed mode I and II loading. Fatigue Fract Eng Mater Struct 1992;15:965.
[14] Christensen RH. Fatigue crack growth affected by metal fragments wedged between opening-closing crack surfaces. Appl Mater Res 1963;2:207.
[15] Elber W. Fatigue crack closure under cyclic tension. Eng Fract Mech 1970;2:37.

[16] Elber W. The significance of fatigue crack closure. ASTM Special Technical Publication; 1971. p. 230.
[17] McClung RC, Sehitoglu H. On the finite element analysis of fatigue crack closure. 1. Basic modeling issues. Eng Fract Mech 1989;33:237.
[18] McClung RC, Sehitoglu H. On the finite element analysis of fatigue crack closure. 2. Numerical results. Eng Fract Mech 1989;33:253.
[19] Allison JE, Ku RC, Pompetzki MA. A comparison of measurement methods and numerical procedures for the experimental characterization of fatigue crack closure. In: Mechanics of fatigue crack closure, ASTM STP 982. Philadelphia, PA: American Society of Testing and Materials; 1988. p. 171–85.
[20] Schijve J. Fatigue crack closure: observations and technical significance. In: Mechanics of fatigue crack closure, ASTM STP 982. Philadelphia, PA: American Society of Testing and Materials; 1988. p. 5–34.
[21] Sehitoglu H. Crack opening and closure in fatigue. Eng Fract Mech 1985;21:329.
[22] Macha DE, Corbly DM, Jones JW. On the variation of fatigue-crack-opening load with measurement location. Exp Mech 1979;19:207.
[23] Riddell WT, Piascik RS, Sutton MA, Zhao W, McNeill SR, Helm JD. Determining fatigue crack opening loads from near-crack-tip displacement measurements. San Diego, CA, USA: ASTM; 1999. p. 157.
[24] Sutton MA, Zhao W, McNeill SR, Helm JD, Piascik RS, Riddell WT. Local crack closure measurements: development of a measurement system using computer vision and a far-field microscope. San Diego, CA, USA: ASTM; 1999. p. 145.
[25] Williams D, Davidson D, Lankford J. Fatigue-crack-tip plastic strains by the stereoimaging technique. Exp Mech 1980;20:134.
[26] McClung RC, Davidson DL. High resolution numerical and experimental studies of fatigue cracks. Eng Fract Mech 1991;39:113.
[27] Carroll J, Efstathiou C, Lambros J, Sehitoglu H, Hauber B, Spottswood S, et al. Investigation of fatigue crack closure using multiscale image correlation experiments. Eng Fract Mech 2009;76:2384.
[28] Sadananda K, Glinka G. Dislocation processes that affect kinetics of fatigue crack growth. Philos Mag 2005;85:189.
[29] Mughrabi H. Cyclic slip irreversibilities and the evolution of fatigue damage. Metall Mater Trans B: Process Metall Mater Process Sci 2009;40:431.
[30] Wu XJ, Koul AK, Krausz AS. A transgranular fatigue crack growth model based on restricted slip reversibility. Metall Trans A (Phys Metall Mater Sci) 1993;24A:1373.
[31] Deshpande VS, Needleman A, Van Der Giessen E. A discrete dislocation analysis of near-threshold fatigue crack growth. Acta Mater 2001;49:3189.
[32] Brinckmann S, Siegmund T. Computations of fatigue crack growth with strain gradient plasticity and an irreversible cohesive zone model. Eng Fract Mech 2008;75:2276.
[33] Karaman I, Sehitoglu H, Maier HJ, Chumlyakov YI. Competing mechanisms and modeling of deformation in austenitic stainless steel single crystals with and without nitrogen. Acta Mater 2001;49:3919.
[34] Tada H, Paris PC, Irwin GR. The stress analysis of cracks handbook. 2nd ed. St. Louis, MO; 1985.
[35] Sih GC, Paris PC, Irwin GR. On cracks in rectilinearly anisotropic bodies. Int J Fract Mech 1965;1:189.
[36] Rice JR. Mechanics of crack tip deformation and extension by fatigue. ASTM STP 1967;415:247.
[37] Hirth JP, Lothe J. Theory of dislocations. 2nd ed. New York: Wiley Interscience; 1992.
[38] Sun W, Sehitoglu H. Residual stress fields during fatigue crack growth. Fatigue Fract Eng Mater Struct 1992;15:115–28.